Quantitative "Magnetic Resonance Immunohistochemistry" with Ligand-Targeted ^{19}F Nanoparticles

Anne M. Morawski,[1] Patrick M. Winter,[1] Xin Yu,[1] Ralph W. Fuhrhop,[1] Michael J. Scott,[1] Franklin Hockett,[1] J. David Robertson,[2] Patrick J. Gaffney,[3] Gregory M. Lanza,[1] and Samuel A. Wickline[1*]

Unstable atherosclerotic plaques exhibit microdeposits of fibrin that may indicate the potential for a future rupture. However, current methods for evaluating the stage of an atherosclerotic lesion only involve characterizing the level of vessel stenosis, without delineating which lesions are beginning to rupture. Previous work has shown that fibrin-targeted, liquid perfluorocarbon nanoparticles, which carry a high payload of gadolinium, have a high sensitivity and specificity for detecting fibrin with clinical ^{1}H MRI. In this work, the perfluorocarbon content of the targeted nanoparticles is exploited for the purposes of ^{19}F imaging and spectroscopy to demonstrate a method for quantifiable molecular imaging of fibrin in vitro at 4.7 T. Additionally, the quantity of bound nanoparticles formulated with different perfluorocarbon species was calculated using spectroscopy. Results indicate that the high degree of nanoparticle binding to fibrin clots and the lack of background ^{19}F signal allow accurate quantification using spectroscopy at 4.7 T, as corroborated with proton relaxation rate measurements at 1.5 T and trace element (gadolinium) analysis. Finally, the extension of these techniques to a clinically relevant application, the evaluation of the fibrin burden within an ex vivo human carotid endarterectomy sample, demonstrates the potential use of these particles for uniquely identifying unstable atherosclerotic lesions in vivo. Magn Reson Med 52:1255–1262, 2004. © 2004 Wiley-Liss, Inc.

Key words: magnetic resonance imaging; molecular imaging; contrast agents; nanoparticles; fibrin; fluorine

Atherosclerotic plaque progresses in discrete stages, entailing multiple episodes of rupture and healing that ultimately culminate in a complete obstruction, leading to an acute heart attack or stroke (1). Regardless of the cellular and molecular mechanisms responsible for destabilization of plaques, microdeposits of fibrin are the hallmark, or the sine qua non, of the unstable lesion, as shown originally by Constantinides, who documented microfissures in unstable plaques in pathologic human arterial specimens (2). Plaques populate the arterial system in a multiplicity of stages, which complicates the task of defining those that are most dangerous, much less identifying the elusive "culprit lesion" (3,4). Unfortunately, traditional methods of screening for such lesions (e.g., cardiac catheterization, CT, ultrasound, magnetic resonance angiography) are incapable of characterizing microfissures that might presage catastrophic plaque rupture.

Vascular endothelium that exhibits fibrin deposits is pathologic, because such deposits are undeniable evidence of either plaque rupture or endothelial erosion, either of which may be a direct precursor of catastrophic occlusion (5). Numerous cellular and molecular processes may play a role in creating vulnerable and ultimately unstable plaques including: (1) macrophages and other inflammatory cells accumulating at the shoulders of plaque caps, which secrete matrix metalloproteinases (MMPs) that can dissolve fibrous components of the cap (6,7); (2) large lipid cores that induce prothrombotic tissue factor (8) and destabilize lesions by distributing stress to rupture-prone shoulder regions (9); (3) apoptosis of smooth muscle cells that destabilizes the structure of plaque caps (10); and (4) lesion angiogenesis (11,12). A substantial amount of research continues to be devoted to the basic science and the clinical detection of these factors involved in the evolution of vulnerable plaques. However, we have chosen to focus on the unstable rather than the vulnerable lesion because these microfissured lesions have already declared themselves as harbingers of clinical events, and sensitive detection of impending rupture could directly and immediately impact therapeutic strategies.

To sensitively diagnose unstable plaques in vivo, we have developed a noninvasive molecular imaging approach that utilizes a highly potent and specific ligand-targeted magnetic resonance (MR) contrast agent for detection of small concentrations of fibrin in unstable lesions with the use of routine magnetic resonance imaging (MRI) at 1.5 T. This unique paramagnetic contrast agent is composed of lipid-encapsulated, liquid perfluorocarbon nanoparticles that can be formulated with a large number of chelated gadolinium atoms (>50000) situated in the bounding lipid, thereby dramatically enhancing local R_1 relaxation rates (13,14). Particle targeting is accomplished with the use of highly specific monoclonal antibody ligands and leads to localization of the MR signal amplification to the area of pathology with little or no competing blood pool signal. This nanosystem can be used for in vivo

[1]Cardiovascular MR Laboratories, Department of Medicine and Department of Biomedical Engineering, Washington University, Saint Louis, Missouri.

[2]Analytical Chemistry Group, University of Missouri Research Reactor, Columbia, Missouri.

[3]St. Thomas' Hospital, London, UK.

Grant sponsor: National Institutes of Health; Grant numbers: HL-42950, HL-59865, EB-01704, and NO1-CO-07121; Grant sponsor: American Heart Association; Grant sponsor: Philips Medical Systems.

Drs. Morawski and Winter contributed equally to the work.

*Correspondence to: Samuel A. Wickline, Washington University School of Medicine, Campus Box 8086, 660 South Euclid Avenue, St. Louis, MO 63110. E-mail: saw@howdy.wustl.edu, Web: http://cmrl.wustl.edu

Received 11 March 2004; revised 27 July 2004; accepted 27 July 2004.

DOI 10.1002/mrm.20287

Published online in Wiley InterScience (www.interscience.wiley.com).

Table 1
Physical and chemical properties for the nanoparticle formulations used in this study

	A	B	C	D
Core component	Perfluoro-15-crown-5	Safflower oil	PFOB[a]	PFOB[a]
Gadolinium chelate	Gd-DTPA-BOA[b]	N/A	Gd-DPTA-BOA[b]	Gd-DTPA-PE[c]
Particle diameter (nm)	193	192	206	261
Particle concentration (nM)*	106.7	98.5	87.7	78.7
^{19}F concentration (M)*	11.7	0	13.1	13.1

[a]Perfluorooctylbromide (perflubron).
[b]Gadolinium-diethylene-triamine-pentaacetic acid-bis-oleate.
[c]Gadolinium-diethylene-triamine-pentaacetic acid-phosphatidylethanolamine.
*Concentration given with respect to total emulsion volume.

targeting of a variety of epitopes, including fibrin, $\alpha_n\beta_3$-integrin, and tissue factor, and has demonstrated a high degree of sensitivity and specificity for detection at clinical field strengths (13–15).

We recently proposed and validated convenient methods for image-based computation of the concentration of targeted molecular epitopes based on the measured T_1 relaxation induced by the paramagnetic particles, which corresponds directly to the local concentration of gadolinium atoms, and hence the concentration of bound nanoparticles (16). However, first generation contrast agents that depend on alterations in proton T_1 and T_2/T_2^* signals could be susceptible to the physiologically heterogeneous distribution of local proton density, signal strength, and magnetic field inhomogeneities, which could vary enough from voxel to voxel to complicate both the detection and the quantification of molecular epitopes based solely on such measurements. Fortunately, the perfluorocarbon core of the nanoparticles serves as a unique tracer for delineating the presence and concentration of bound nanoparticles, because living organisms contain practically no detectable amounts of fluorine under in vivo imaging conditions.

While MR techniques are almost as sensitive to fluorine as they are to protons because of their high gyromagnetic ratios, the relative lack of fluorine-containing compounds in vivo has limited the clinical applicability of this technique. However, ^{19}F MRI has been used for a variety of research applications including studying tumor metabolism (17–19), mapping physiologic pO_2 in various tissues (20–23), quantifying albumin concentration (24), and mapping liquid ventilation (25,26). To overcome the limited abundance of fluorine-containing compounds in vivo, many of these studies were performed at high magnetic fields, 4.7 T or greater (21–23,25,27), and/or they increased the concentration of ^{19}F via direct injection or physiologic replacement (21,25,26). For targeted perfluorocarbon nanoparticles, the binding of the agent to the tissue or epitope of interest serves to increase the concentration of fluorine in that area to a level that allows ^{19}F spectroscopy and imaging within a reasonable scan time.

Accordingly, we hypothesized that ^{19}F spectroscopy and/or imaging could yield highly specific and quantitative information regarding the concentration of nanoparticles bound to targeted pathologic molecules. In particular, we sought to determine whether ^{19}F spectroscopy and imaging could be utilized to quantify molecular binding of fibrin-targeted nanoparticles to samples known to contain fibrin, human plasma clots, and an ex vivo carotid endarterectomy specimen (28). Furthermore, we aimed to utilize the unique spectral patterns of different perfluorocarbon core materials to distinguish two species of targeted nanoparticles. Successful realization of these goals would establish an approach for robust quantification of one or multiple pathologic molecular epitopes using MRI.

METHODS

Nanoparticle Formulations

Four biotinylated nanoparticle emulsions (Table 1) were formulated as described previously (13). Briefly, they were composed of 20% (v/v) of a core component, 2% (w/v) safflower oil, 2% (w/v) of a surfactant comixture, and 1.7% (w/v) glycerin, with water comprising the balance. The core component was: (1) perfluorooctylbromide (PFOB; Minnesota Manufacturing and Mining, St. Paul, MN), also known as perflubron, (2) perfluoro-15-crown-5 (Exfluor Research Corp., Round Rock, TX), or (3) safflower oil. The nonparamagnetic safflower oil particles were formulated with a surfactant comixture containing 70 mol% lecithin (Avanti Polar Lipids, Inc., Alabaster, AL), 28 mol% cholesterol (Sigma Chemical Co., St. Louis, MO), and 2 mol% biotinylated dipalmitoyl-phosphatidylethanolamine (Avanti Polar Lipids, Inc.). The paramagnetic agents were formulated with 30 mol% of a lipophilic gadolinium chelate in the surfactant comixture accompanied by equivalent decreases in lecithin (60 mol%) and cholesterol (8 mol%). The crown ether and one of the PFOB emulsions were produced with gadolinium-diethylene-triamine-pentaacetic acid-bis-oleate (Gd-DTPA-BOA; Gateway Chemical Technologies, St. Louis, MO) (29). The other PFOB emulsion was formulated with Gd-DTPA-phosphatidylethanolamine (Gd-DTPA-PE; Gateway Chemical Technologies), which provides higher intrinsic relaxivity (14).

Particle sizes were determined at 25°C with a laser light scattering submicrometer particle sizer (Malvern Instruments, Malvern, Worcestershire, UK). The concentration of nanoparticles was derived from the nominal particle size (i.e., volume of a sphere) and the amount of core perfluorocarbon component formulated into the preparation according to the formula

$$[\mathrm{NP}] = \frac{V_{\mathrm{NP}}}{v_{\mathrm{np}} \cdot V_{\mathrm{E}} \cdot N_{\mathrm{av}}},$$

where V_{NP} is the total volume of the components used to create the nanoparticles (safflower oil, perfluorocarbon, and surfactant layer), v_{np} is the volume of each nanoparticle, assumed to be a sphere, using the measured particle size, V_E is the total volume of the final emulsion, and N_{av} is Avogadro's number.

Nanoparticle Phantom ^{19}F Spectroscopy

Two PFOB emulsions which incorporated gadolinium chelates with vastly different relaxivities, Gd-DTPA-BOA or Gd-DTPA-PE (14), were diluted to 10, 15, 20, 25, and 30% (v/v) with distilled deionized water. Fluorine free induction decays were measured for each sample with a Bruker Minispec at 0.47 T (4096 points, 20-kHz sweep width, 5-sec pre-delay, 128 averages) and Fourier transformed using the associated ExpSpel software to obtain ^{19}F NMR spectra. The signal intensity was integrated and normalized with respect to a standard composed of reagent grade PFOB. The ^{1}H r_1 relaxivities measured for the Gd-DTPA-BOA and Gd-DTPA-PE emulsions at 0.47 T were 21.3 and 36.9 $(\text{sec}\cdot\text{mM})^{-1}$, respectively (14).

Fibrin-Targeted Clots and Ex Vivo Human Carotid Arteries

Fresh-frozen human plasma anticoagulated with sodium citrate was used to form fibrin clots by combining plasma, 100 mM calcium chloride (3:1 v/v), and 5 U thrombin (Dade Behring, Germany) in the bottom of plastic sample vials. A human carotid endarterectomy sample was obtained postsurgically from a symptomatic patient and frozen until treatment. After being thawed, the carotid artery was rinsed with sterile saline to remove residual blood. The artery and in vitro clots were serially incubated with 125 μg biotinylated anti-fibrin monoclonal antibody (30) (NIB 1H10) overnight at 4°C, followed by 125 μg avidin for 1 hr at 37°C, and then 100 μL of the selected biotinylated nanoparticles for 1 hr at 37°C to complete the binding. All samples were rinsed three times with sterile saline after each incubation step to remove any unbound reactants. Following the last incubation step, the fibrin clots were covered in agarose.

In vitro competition experiments were performed to vary the concentrations of signal-generating nanoparticles bound to the clots (and hence MR signal) by combining admixed volumes of paramagnetic fluorinated agent (column A from Table 1) with the nonfluorinated nonparamagnetic safflower oil agent (column B) in ratios of 0:1, 1:3, 1:1, 3:1, and 1:0. The oil nanoparticles were designed to compete for fibrin binding but not exhibit a ^{19}F MR signal or ^{1}H signal enhancement. A second set of mixtures was created to generate two different fluorine signals from the same clot. These were produced by combining different volumes of paramagnetic PFOB (column C) and crown ether nanoparticles (column A), also in ratios of 0:1, 1:3, 1:1, 3:1, and 1:0 respectively. Each of the 10 formulations was applied to three separate clots. The carotid artery was treated with paramagnetic crown ether nanoparticles (column A) only.

MR Spectroscopy and Imaging of Clot and Carotid Samples

All ^{19}F spectra and images were collected on a 4.7-T Varian Inova with a 3.5-cm-long by 2-cm-diameter loop–gap resonator tunable to 200 MHz for ^{1}H or 188 MHz for ^{19}F. An external standard of NMR-grade trichlorofluoromethane (CFC-11; Sigma Chemical Co.) was affixed to the coil during all spectroscopic experiments. Fluorine spectra (50-kHz sweep width; 32768 points; ~12-min scan time; 90° flip angle; 128 acquisitions; 5-sec pre-delay) were acquired from selected volumes of undiluted crown ether (0, 1.5, 2, 4, and 10 μL) and PFOB nanoparticles (0, 1.5, 2, and 4 μL) to generate a calibration curve for fluorine quantification. After applying 30 Hz line broadening, the largest PFOB peak and the single crown ether peak were integrated with respect to the CFC-11 peak using Nuts NMR (Acorn NMR, Inc., Livermore, CA). The integrated values were plotted against the amount of perfluorocarbon in each sample and fit using linear regression. Since the longitudinal relaxation times at 4.7 T for the PFOB and crown ether nanoparticles are estimated to be 1.65 and 0.93 sec, respectively, no corrections were applied to the integrated values to compensate for partial-saturation effects (31,23). Fluorine spectra from each clot and the carotid artery were acquired and integrated in an identical fashion. The integrated ^{19}F signal and the calibration curves were used to calculate the number of particles bound to each sample.

A clot treated with the paramagnetic crown ether agent was also imaged at 4.7 T with a multislice spin echo sequence (256 × 256 matrix; 1.0 sec TR; 7.3 msec TE; 7 slices; 3 × 5 mm field of view; 2 mm slice thickness; 1 acquisition; ~5 min acquisition time) with the same coil used to acquire the spectra. Both proton density weighted ^{1}H and ^{19}F images were collected to colocalize the fluorine signal with the ^{1}H signal. All clots treated with the crown ether and oil formulations were imaged at 1.5 T (NT Intera CV, Philips Medical Systems, Best, Netherlands) to obtain proton T_1 maps using a quadrature birdcage receiver coil and a mixed spin echo and inversion recovery sequence (0.23 × 0.23 × 2 mm resolution; 19 msec TE; 760 msec spin echo TR; 2.3 sec inversion recovery TR; 370 msec inversion recovery delay; ~4 hr acquisition time) (32).

The carotid endarterectomy sample was imaged at 4.7 T using both ^{1}H and ^{19}F MRI for detection of fibrin-targeted nanoparticles. Multislice spin echo ^{1}H images were acquired for localization prior to obtaining a spin echo projection ^{19}F image (64 × 32 matrix; 1.0 sec TR; 4.5 msec TE; 1 slice; 3 × 3 mm field of view; 26 mm slice thickness; 2 signal averages).

Neutron Activation Analysis for Gd^{3+} Content

The gadolinium content of the fibrin clot samples was analyzed by standard neutron activation techniques conducted at the Research Reactor facility at the University of Missouri (MURR) (33). After lyophilization, the mass of gadolinium was calculated from the beta decay of ^{161}Gd produced through neutron capture on ^{160}Gd. Individual samples and standards were irradiated in a thermal neutron flux of about 5×10^{13} $\text{n}\cdot\text{cm}^{-2}\cdot\text{sec}^{-1}$ for 7 sec, allowed to decay for 30 sec, and counted on a high-resolution γ-ray spectrometer for 300 sec.

RESULTS

Nanoparticle Characteristics

All four nanoparticle emulsions had nominal particle diameters around 200–300 nm, regardless of the core component or the incorporation of a paramagnetic chelate (Table 1). Other physical properties, such as particle and fluorine concentrations, were also very similar for each formulation (Table 1).

Effect of Gadolinium Chelates on ^{19}F Spectroscopy

The ^{19}F signal acquired at 0.47 T from PFOB nanoparticles formulated with Gd-DTPA-BOA or Gd-DTPA-PE is linear with respect to fluorine content (Fig. 1). Additionally, the two regression lines are statistically identical, indicating that the incorporation of a paramagnetic chelate into the nanoparticle membrane does not affect the ^{19}F signal from the perfluorocarbon core.

Quantification of Signal from Fibrin-Targeted Clots

At 4.7 T, the ^{19}F spectrum from crown ether nanoparticles consisted of a single peak, clearly separated −90 ppm from the trichlorofluoromethane signal (Fig. 2a). This single crown ether peak is particularly attractive for maximizing the signal-to-noise in fluorine spectra and images. The relative crown ether signal intensity (with respect to the trichlorofluoromethane peak) from known emulsion volumes provided a calibration curve for nanoparticle quantification (Fig. 2b). A similar calibration curve was obtained from the PFOB agent (not shown). These calibration curves allowed quantification of the number of nanoparticles bound to each fibrin clot and the carotid endarterectomy segment using the fluorine signal.

Human plasma clots treated with a mixture of paramagnetic crown ether and nonparamagnetic safflower oil nanoparticles provided two means for quantifying the number of bound fibrin-targeted nanoparticles: the ^{19}F signal from the crown ether core and neutron activation analysis of the gadolinium on the particle surface. Both the ^{19}F signal and the gadolinium content decreased linearly as the amount of competing safflower oil agent was increased. As expected, the number of bound paramagnetic fluorinated nanoparticles, as calculated from the normalized ^{19}F spectroscopic signal, is directly proportional to the measured gadolinium content of the clots (Fig. 2c). Treatment with the undiluted crown ether emulsion provided a high number of bound nanoparticles, each composed of a large amount of perfluorocarbon, allowing acquisition of high signal-to-noise ratio (20.8) fluorine im-

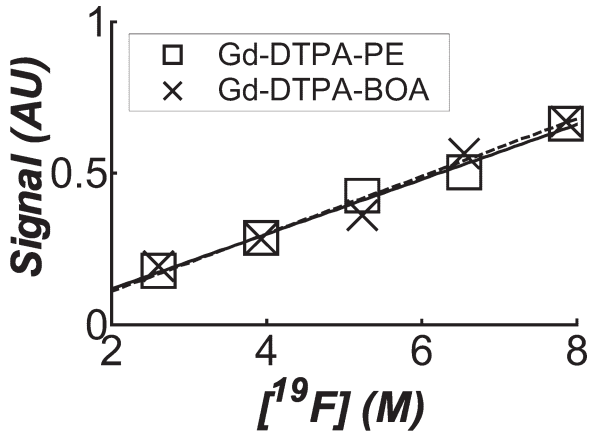

FIG. 1. Fluorine spectral signal intensity acquired at 0.47 T for two paramagnetic PFOB nanoparticle emulsions formulated with different lipophilic paramagnetic chelates. Signal intensity is linear with respect to fluorine concentration for nanoparticles formulated with either gadolinium-DTPA-bis-oleate (Gd-DTPA-BOA) or gadolinium-DTPA-phosphatidylethanolamine (Gd-DTPA-PE).

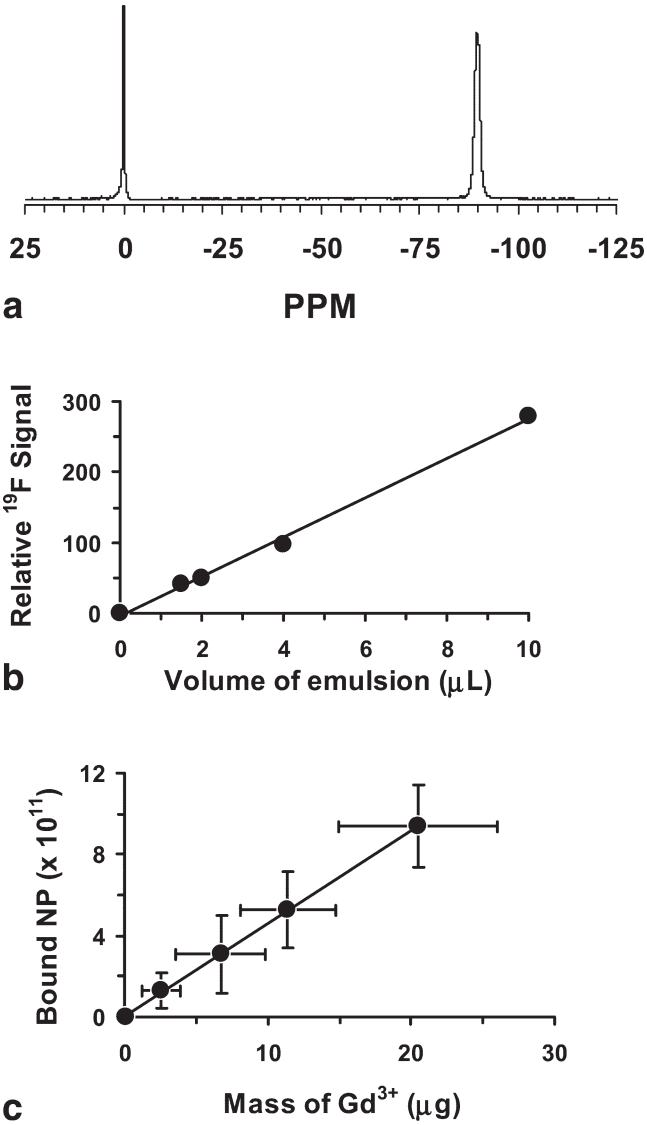

FIG. 2. (**a**) Representative spectrum taken at 4.7 T of crown ether emulsion (−90 ppm) and trichlorofluormethane (0 ppm) used as a reference. (**b**) The calibration curve for crown ether emulsion has a slope and intercept of 28.06 and −4.86, respectively, with an $r^2 > 0.99$. A similar calibration curve for the PFOB emulsion (not shown) was obtained (slope = 5.01, intercept = 0.06, $r^2 > 0.99$). (**c**) The calculated number of bound nanoparticles (means ± SE) as determined from ^{19}F spectroscopy and the mass of total gadolinium (Gd^{3+}) in the sample as evaluated with neutron activation analysis show excellent agreement as independent measures of fibrin-targeted nanoparticle binding to clots ($r^2 > 0.99$).

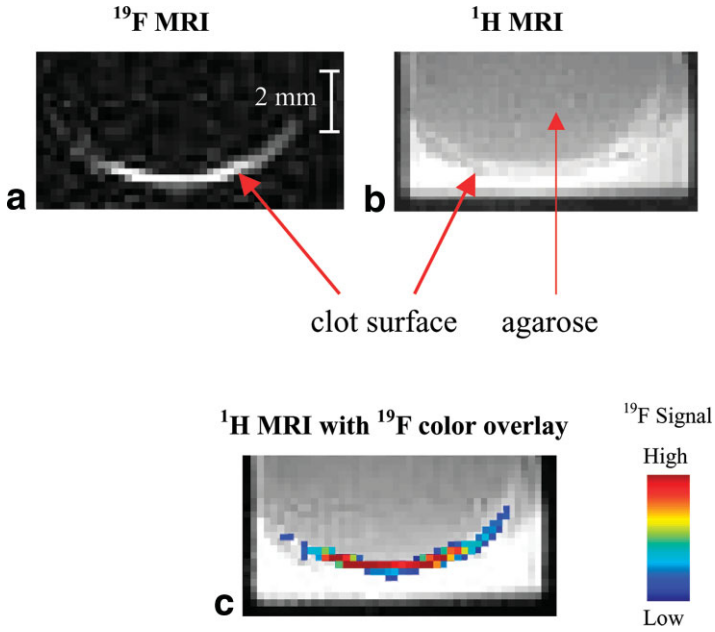

FIG. 3. (**a**) ^{19}F image (4.7 T) of a single slice through a clot treated with crown ether emulsion. High signal is observed at the clot surface due to bound fluorinated nanoparticles. (**b**) ^{1}H image (4.7 T) of the same slice showing the anatomy of the clot. (**c**) False color overlay of ^{19}F signal onto ^{1}H image clearly showing localization of ^{19}F signal to the clot surface.

ages at 4.7 T in less than 5 min (Fig. 3a). A corresponding ^{1}H image of the same slice showed that the ^{19}F signal from the bound nanoparticles was localized to the clot surface (Fig. 3b and c).

Proton longitudinal relaxation rates (R_1) measured at 1.5 T provided another method for quantification of fibrin-targeted crown ether nanoparticles on the clots. The R_1 maps clearly illustrated increased relaxation rates at the clot surface with increasing amounts of gadolinium in the admixed formulations (Fig. 4a). In addition, the increased proton relaxation rate was correlated with the gadolinium content as measured by neutron activation analysis (Fig. 4b).

Clots treated with the mixtures of crown ether and PFOB nanoparticles exhibited two distinct fluorine signals that were easily differentiated with spectroscopy at 4.7 T (Fig. 5a). Spectral analysis showed that the relative binding of the two nanoparticle species was highly related to the ratio of PFOB to crown ether emulsion applied (Fig. 5b).

An optical image of the human carotid endarterectomy sample revealed extensive wall thickening, lipid deposition, and plaques of heterogeneous nature (Fig. 6a), as has been previously documented for these samples (34,35). A ^{19}F projection image of the artery was acquired in less than 5 min, showing an asymmetric distribution of fibrin targeted nanoparticles around the vessel wall (Fig. 6b). Spec-

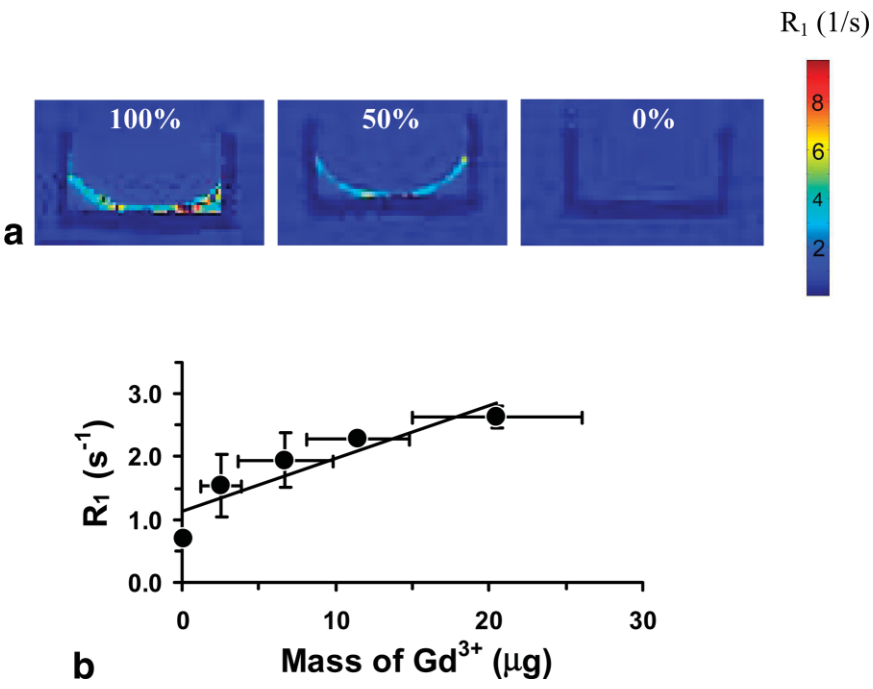

FIG. 4. (**a**) R_1 proton relaxation rate maps of three representative targeted clots at 1.5 T. (**b**) The proton relaxation rate (R_1) of the clots at 1.5 T correlates with the gadolinium content as measured with neutron activation (means ± SE; $r^2 = 0.83$).

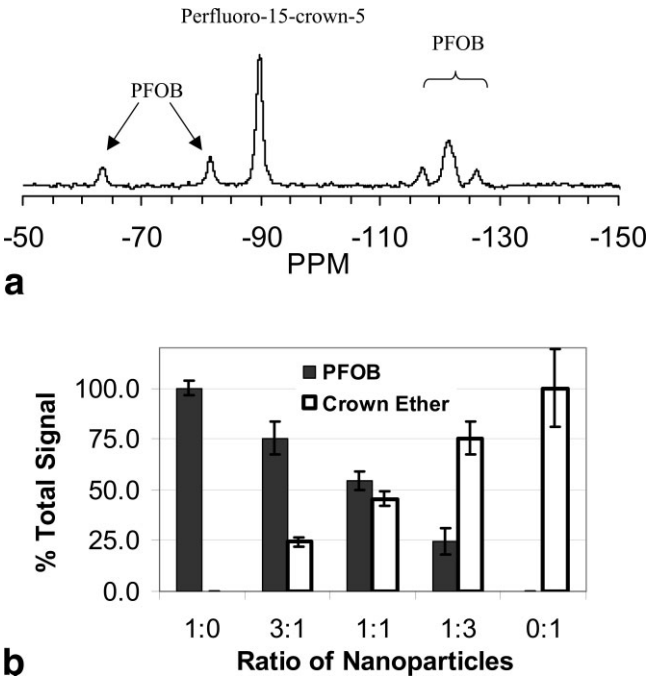

FIG. 5. (**a**) Representative ^{19}F spectrum acquired at 4.7 T of a clot treated with a mixture of fibrin-targeted crown ether and PFOB emulsions. The crown ether peak and five discernible PFOB peaks are easily detected and individually resolved. (**b**) Percentage of total ^{19}F signal attributed to crown ether or PFOB for the clots treated with different nanoparticle mixtures ($n = 3$; plotted as means ± SE). Emulsion mixtures are listed as the ratio of PFOB to crown ether. Spectral discrimination of crown ether and PFOB allows quantification of the two nanoparticle species within a single sample.

troscopic quantification of nanoparticle binding allowed calibration of the ^{19}F MRI signal intensity. The quantitative nanoparticle map, together with ^{1}H images, permits visualization of anatomic and definitive pathologic information with MRI (Fig. 6c).

DISCUSSION

A potential key application for targeted diagnostic nanotechnologies is the identification of "preclinical" atherosclerosis. Indeed, of the 720000 deaths per year in America attributed to heart disease, 60% are classified as "sudden deaths," which occur without premonitory warning signs (36). This figure suggests that current diagnostic strategies are inadequate for identifying patients who are most susceptible to infarction and death *at any stage* in the development of atherosclerosis lesions. To address this need, fibrin-targeted nanoparticles were developed as an analog to traditional immunocytochemistry to enable absolute quantification of the concentration of certain pathologic epitopes in vivo with MRI methods that should be directly applicable to patients.

The present data illustrate the following new findings: (1) spectroscopy enables ready detection of molecular binding based on registration of the unique fluorine signal associated with these nanoparticle contrast agents; (2) the concentration of targeted nanoparticles, and hence fibrin epitopes, can be quantified based on the fluorine spectral signatures; (3) distinct species of nanoparticles formulated with different perfluorocarbon core components can be identified; and (4) these techniques can be applied to clinically relevant situations. To our knowledge, these are the first molecular imaging applications for MRI that establish the possibility of unambiguous quantification of the concentration of specific molecular epitopes with the use of targeted contrast agents. Heretofore, single image-based quantification has been an advantage of nuclear or PET imaging technologies, but MRI in concert with targeted molecular contrast agents with unique signatures may open a new field of high-resolution quantitative imaging of molecules of pathologic importance with the use of nonradioactive molecular tracer elements.

With the use of several different nanoparticle formulations, we verify the relationship between the extent of nanoparticle binding and the ^{19}F signal quantified from spectroscopy, as well as the ^{1}H signal enhancement from gadolinium quantified from its T_1 effect (16). The concomitant application of these two imaging modes creates a synergistic molecular imaging approach that might comprise an initial rapid, low resolution scan to identify areas of gadolinium enhancement in the volume of interest and then more localized ^{19}F spectroscopy or imaging for quantification of unique signals from specific molecules. Because atherosclerosis is characterized by the presence of multiple vulnerable lesions (3,4), this technique would allow delineation of those most prone to untoward clinical events due to excessive fibrin deposits on plaques with microfissuring. Together, the use of both ^{1}H MRI and ^{19}F

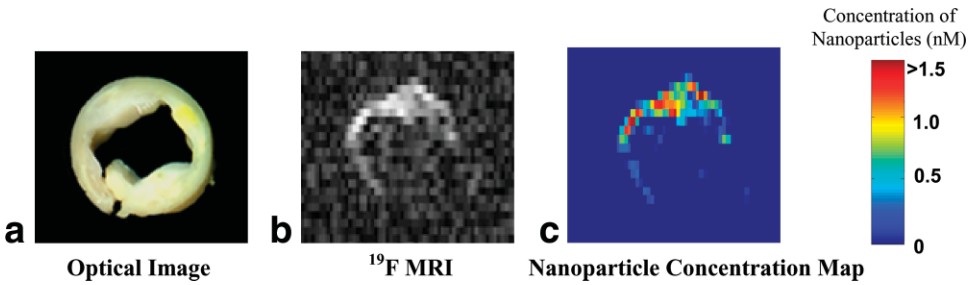

FIG. 6. (**a**) Optical image of a 5-mm cross-section of a human carotid endarterectomy sample. This section showed moderate lumenal narrowing as well as several atherosclerotic lesions. (**b**) A ^{19}F projection image acquired at 4.7 T through the entire carotid artery sample shows high signal along the lumen due to nanoparticles bound to fibrin. (**c**) Concentration map of bound nanoparticles in the carotid sample.

imaging and spectroscopy offers synergies for enhancing clinical treatment strategies.

In addition, we demonstrate a potential method for multiple epitope detection by registering nanoparticles with different perfluorocarbon cores (Fig. 5). Because the composition of atherosclerotic lesions influences their potential for future rupture, noninvasive methods for differentiating high-risk plaques have been developed that use various imaging modalities including ^{1}H MRI (37,38,35). These methods generally characterize lesion composition and geometry, such as the size of the lipid core or the thickness of the fibrous cap, rather than addressing molecular markers of disease activity such as fibrin deposition or cellular events involved in the inflammation. Identification of distinct perfluorocarbons in particles separately targeted to individual molecules with the use of broadband ^{19}F spectroscopy would enable simultaneous objective exploration of a variety of cellular epitopes within the same area of pathology. Thus, direct detection and quantification of the spatial and temporal interaction of multiple molecular factors could provide insight into how they operate in concert to cause a particular disease process such as atherosclerosis.

Finally, we demonstrate the application of these techniques to a clinically significant example, a diseased, human carotid artery segment imaged ex vivo. These results indicate that paramagnetic fluorinated nanoparticles create visually apparent contrast on proton MR images as well as ample signal-to-noise on ^{19}F MR images at clinically relevant concentrations due to the high payload of gadolinium and crown ether within each particle. Additionally, we demonstrate that ^{19}F spectroscopy and imaging can be combined to generate quantitative maps of the location and concentration of pathologic molecules within a sample. The application of this technique to the carotid artery sample yielded nanoparticle concentrations consistent with previous predictions for the level of binding needed to generate adequate contrast on ^{1}H images (16).

Other epitope-specific contrast agents for MRI are currently under development that are designed to generate bright areas or signal voids that correspond to the targeted tissue on ^{1}H images. One such fibrin-specific agent is being used for the characterization and identification of plaque rupture and subsequent thrombus with the use of gadolinium chelates for hot-spot ^{1}H MRI (39). Although this agent harbors a much smaller payload of gadolinium than do the perfluorocarbon nanoparticles, the epitope density for fibrin in larger blood clots appears sufficient to produce a reasonable change in MR signal. As an alternative method for visualizing specific cells and tissues, other researchers have developed superparamagnetic iron oxide particles that are selectively taken up by cells transfected to express high levels of the targeted receptor, thereby reducing the signal generated in these areas on T_2^*-weighted images (40). While both of these agents can be quantified using R_1 or R_2 relaxation rate changes on ^{1}H images, the ^{19}F signal from the perfluorocarbon nanoparticles provides unique and unequivocal confirmation of targeting and direct quantification of binding.

However, certain challenges exist for the clinical application of ^{19}F spectroscopy and imaging. First, the fluorine signal is intrinsically weak as compared with that of protons in view of their limited concentration. To be clinically applicable, ^{19}F imaging of targeted nanoparticles must be possible at 1.5 or 3.0 T. Previous studies have reported the minimum detectable limit of ^{19}F at 1.5 T is 30 μM (18). This concentration is difficult to achieve with a circulating agent that might passively accumulate at a selected site in vivo. Targeted perfluorocarbon nanoparticles, however, might overcome this limitation, because the specific binding permits local accumulation of nanoparticles at the site of pathology (up to 1 nM concentration as shown in Fig. 6c), and each individual nanoparticle carries an extremely high payload of fluorine (12–13 M from Table 1). These factors allow us to accumulate ^{19}F at the plaque surface to a concentration > 0.1 M, which is well above the reported minimum detection limit. Therefore, we suggest that molecular imaging and quantitative ^{19}F spectroscopy and imaging should be clinically feasible at 1.5 T.

ACKNOWLEDGMENTS

The authors thank Dr. Joseph J. H. Ackerman, Professor and Chair, Department of Chemistry, and Director of the Biomedical MR Laboratory at Washington University, for technical assistance and support. We are grateful to Gregorio A. Sicard, M.D., for providing the human carotid endarterectomy samples.

REFERENCES

1. Ojio S, Takatsu H, Tanaka T, Ueno K, Yokoya K, Matsubara T, Suzuki T, Watanabe S, Morita N, Kawasaki M, Nagano T, Nishio I, Sakai K, Nishigaki K, Takemura G, Noda T, Minatoguchi S, Fujiwara H. Considerable time from the onset of plaque rupture and/or thrombi until the onset of acute myocardial infarction in humans: coronary angiographic findings within 1 week before the onset of infarction. Circulation 2000; 102:2063–2069.
2. Constantinides P. Plaque fissuring in human coronary thrombosis. J Atheroscler Res 1966;6:1–17.
3. Goldstein JA. Angiographic plaque complexity: the tip of the unstable plaque iceberg. J Am Coll Cardiol 2002;39:1464–1467.
4. Goldstein JA. Multifocal coronary plaque instability. Prog Cardiovasc Dis 2002;44:449–454.
5. Virmani R, Burke AP, Kolodgie FD, Farb A. Pathology of the thin-cap fibroatheroma: a type of vulnerable plaque. J Interv Cardiol 2003;16: 267–272.
6. Shah PK. Role of inflammation and metalloproteinases in plaque disruption and thrombosis. Vasc Med 1998;3:199–206.
7. Newby AC, Zaltsman AB. Fibrous cap formation or destruction–the critical importance of vascular smooth muscle cell proliferation, migration and matrix formation. Cardiovasc Res 1999;41:345–360.
8. Petit L, Lesnik P, Dachet C, Moreau M, Chapman MJ. Tissue factor pathway inhibitor is expressed by human monocyte-derived macrophages : relationship to tissue factor induction by cholesterol and oxidized LDL. Arterioscler Thromb Vasc Biol 1999;19:309–315.
9. Arroyo LH, Lee RT. Mechanisms of plaque rupture: mechanical and biologic interactions. Cardiovasc Res 1999;41:369–375.
10. Kockx MM, De Meyer GR, Buyssens N, Knaapen MW, Bult H, Herman AG. Cell composition, replication, and apoptosis in atherosclerotic plaques after 6 months of cholesterol withdrawal. Circ Res 1998;83: 378–387.
11. de Boer OJ, van der Wal AC, Teeling P, Becker AE. Leucocyte recruitment in rupture prone regions of lipid-rich plaques: a prominent role for neovascularization. Cardiovasc Res 1999;41:443–449.
12. McCarthy MJ, Loftus IM, Thompson MM, Jones L, London NJM, Bell PRF, Naylor AR, Brindle NPJ. Angiogenesis and the atherosclerotic carotid plaque: an association between symptomatology and plaque morphology. J Vasc Surg 1999;30:261–268.

13. Flacke S, Fischer S, Scott MJ, Fuhrhop RJ, Allen JS, McLean M, Winter P, Sicard GA, Gaffney PJ, Wickline SA, Lanza GM. Novel MRI contrast agent for molecular imaging of fibrin: implications for detecting vulnerable plaques. Circulation 2001;104:1280–1285.
14. Winter PM, Caruthers SD, Yu X, Song S-K, Fuhrhop RW, Scott MJ, Chen J, Miller B, Bulte JWM, Gaffney PJ, Wickline SA, Lanza GM. Improved molecular imaging contrast agent for early detection of unstable atherosclerotic plaques. Magn Reson Med 2003;50:411–416.
15. Lanza GM, Yu X, Winter PM, Abendschein DR, Karukstis KK, Scott MJ, Fuhrhop RJ, Scherer DE, Wickline SA. Targeted antiproliferative drug delivery to vascular smooth muscle cells with an MRI nanoparticle contrast agent: Implications for rational therapy of restenosis. Circulation 2002;106:2842–2847.
16. Morawski AM, Winter PM, Crowder KC, Caruthers SD, Fuhrhop RJ, Scott MJ, Robertson JD, Abendschein DR, Lanza GM, Wickline SA. Targeted nanoparticles for quantitative imaging of sparse molecular epitopes with MRI. Magn Reson Med 2004;51:480–486.
17. Ikehira H, Girard F, Obata T, Ito H, Yoshitomi H, Miyazaki M, Nakajiman N, Kamei H, Kanazawa Y, Takano H, Tanada S, Sasaki Y. A preliminary study for clinical pharmacokinetics of oral fluorine anticancer medicines using the commercial MRI system 19F-MRS. Br J Radiol 1999;72:584–589.
18. Schlemmer HP, Becker M, Bachert P, Dietz A, Rudat V, Vanselow B, Wollensack P, Zuna I, Knopp MV, Weidauer H, Wannenmacher M, van Kaick G. Alterations of intratumoral pharacokinetics of 5-fluorouracil in head and neck carcinoma during simultaneous radiochemotherapy. Cancer Res 1999;59:2363–2369.
19. Wolf W, Presant CA, Waluch V. ^{19}F-MRS studies of fluorinated drugs in humans. Adv Drug Deliv Rev 2000;41:55–74.
20. Shukla HP, Mason RP, Bansal N, Antich PP. Regional myocardial oxygen tension: ^{19}F MRI of sequestered perfluorocarbon. Magn Reson Med 1996;35:827–833.
21. Le D, Mason RP, Hunjan S, Constantinescu A, Barker BR, Antich PP. Regional tumor oxygen dynamics: ^{19}F PBSR EPI of hexafluorobenzene. Magn Reson Imaging 1997;15:971–981.
22. Noth U, Grohn P, Jork A, Zimmermann U, Haase A, Lutz J. ^{19}F-MRI in vivo determination of the partial oxygen pressure in perfluorocarbon-loaded alginate capsules implanted into the peritoneal cavity and different tissues. Magn Reson Med 1999;42:1039–1047.
23. Fan X, River JN, Zamora M, Al-Hallaq HA, Karczmar GS. Effect of carbogen on tumor oxygenation: combined fluorine-19 and proton MRI measurements. Int J Radiat Oncol Biol Phys 2002;54:1202–1209.
24. Dzik-Jurasz AS, Wolber J, Prock T, Collins DJ, Leach MO, Rowland IJ. The quantitative ^{19}F-image of albumin at 1.5T: a potential in-vivo tool. Magn Reson Imaging 2001;19:839–844.
25. Huang MQ, Ye Q, Williams DS, Ho C. MRI of lungs using partial liquid ventilation with water-in-perfluorocarbon emulsions. Magn Reson Med 2002;48:487–492.
26. Laukemper-Ostendorf S, Scholz A, Burger K, Heussel CP, Schmittner M, Weiler N, Markstaller K, Eberle B, Kauczor HU, Quintel M, Thelen M, Schreiber WG. ^{19}F-MRI of perflubron for measurement of oxygen partial pressure in porcine lungs during partial liquid ventilation. Magn Reson Med 2002;47:82–89.
27. Hunjan S, Zhao D, Canstandtinescu A, Hahan EW, Antich PP, Mason RP. Tumor oximetry: demonstration of an enhanced dynamic mapping procedure using fluorine-19 echo planar magnetic resonance imaging the Dunning prostate R3327-At1 rat tumor. Int J Radiat Oncol Biol Phys 2001;49:1097–1108.
28. Fisher M, Sacoolidge JC, Taylor CR. Patterns of fibrin deposits in carotid artery plaque. Angiology 1987;38:393–399.
29. Cacheris WP, Richard TJ, Grabiek RC, Lee AC, Paramagnetic complexes of *N*-alkyl-*N*-hydroxylamides of organic acids and emulsions containing same for magnetic resonance imaging, in 5,614,170. 1997: USA.
30. Raut S, Gaffney PJ. Evaluation of fibrin binding profile of two antifibrin monoclonal antibodies. Thromb Haemost 1996;76:56–64.
31. Mason RP, Antich PP. Tumor oxygen tension: measurement using Oxygent^{TM} as a ^{19}F NMR proble at 4.7 T. 1994;22:1361–1367.
32. In den Kleef JJ, Cuppen JJ. RLSQ: T1, T2, and rho calculations, combining ratios and least squares. Magn Reson Med 1987;5:513–524.
33. Winter PM, Morawski AM, Caruthers SD, Fuhrhop RW, Zhang H, Williams TA, Allen JS, Robertson JD, Lanza GM, Wickline SA. Molecular imaging of angiogenesis in early-stage atherosclerosis with avb3-integrin-targeted nanoparticles. Circulation 2003;108:2270–2274.
34. Milei J, Parodi JC, Fernandez Alonso G, Barone A, Beigelman R, Ferreira LM, Arrigoni G, Matturri L. Carotid atherosclerosis. Immunocytochemical analysis of the vascular and cellular composition in endarterectomies. Cardiologia 1996;41:535–542.
35. Clarke SE, Hammond RR, Mitchell JR, Rutt BK. Quantitative assessment of cartoid plaque composition using mulitcontrast MRI and registered histology. Magn Reson Imaging 2003;50:1199–1208.
36. Zheng Z-J, Croft JB, Giles WH, Mensah GA. Sudden cardiac death in the United States, 1989 to 1998. Circulation 2001;104:2158–2163.
37. Choudhury RP, Fayad ZA. Imaging of atherosclerosis. Coronary wall imaging with MRI. J Cardiovasc Risk 2002;9:263–270.
38. Nair AN, Kuban BD, Tuzcu EM, Schoenhagen P, Nissen SE, Vince G. Coronary plaque classificiation with intravascular ultrasound radiofrequency data analysis. Circulation 2002;106:2200–2206.
39. Botnar RM, Perez AS, Witte S, Wiethoff AJ, Laredo J, Graham PB, Weisskoff RM, Manning WJ, Johnstone MT. In-vivo molecular imaging of acute and subacute thrombosis using a fibrin binding MRI contrast agent. Circulation 2004;109:2023–2029.
40. Weissleder R, Moore A, Mahmood U, Bhorade R, Benveniste H, Chiocca EA, Basilion JP. In vivo magnetic resonance imaging of transgene expression. Nat Med 2000;6:351–355.